ChemPubSoc Europe

DOI: 10.1002/chem.201405798

CHEMISTRY A European Journal Full Paper

Photoelectrochemical Cytosensor

Long-Lived Charge Carriers in Mn-Doped CdS Quantum Dots for Photoelectrochemical Cytosensing

Peng Wu,[a, b] Jian-Bing Pan,[a] Xiang-Ling Li,[a] Xiandeng Hou,[b] Jing-Juan Xu,*[a] and Hong-Yuan Chen*[a, c]

Abstract: Photoelectrochemical (PEC) biosensing with semiconductor quantum dots (QDs) has received great attention because it integrates the advantages of both photo-excitation and electrochemical detection. During the photon-to-electricity conversion in PEC processes, electron–hole (charge) separation competes with electron–hole recombination, and the net effect essentially determines the performance of PEC biosensors. Herein, we propose a new approach for slowing down electron–hole recombination to increase charge separation efficiency for PEC biosensor development. Through doping with Mn^{2+}, a pair of d bands ($^4T_1$ and $^6A_1$) is inserted between the conduction and valence bands of CdS QDs, which alters the electron–hole separation and recombination dynamics, allowing the generation of long-lived charge carriers with ms-scale lifetime that decay about 10^4–10^5-fold more slowly than in the case of undoped QDs. Photocurrent tests indicated that Mn^{2+} doping resulted in an approximately 80% increase in photocurrent generation compared with undoped CdS QDs. For application, the Mn-doped CdS QDs were coated on the surface of a glassy carbon electrode and functionalized with a cell surface carbohydrate-specific ligand (3-aminophenylboronic acid). In this way, a sensitive cytosensor for K562 leukemia cells was constructed. Moreover, the sugar-specific binding property of 3-aminophenylboronic acid allowed the electrode to serve as a switch for the capture and release of cells. This has been further explored with a view to developing a reusable PEC cytosensing platform.

Introduction

Photoelectrochemical (PEC) biosensors have received a great deal of attention due to their desirable properties and attractive potential in bioassays,[1] with a broad range of analytical targets that includes metal ions,[2] small molecules,[3] DNA,[4] proteins,[5] and cells.[6] Besides, following the discovery of the photoelectric effect by Edmond Becquerel,[7] the exploitation of various functional semiconductive materials for improved PEC performance has long been a focus of research, the most notable materials including porphyrins,[8] TiO_2,[9] CdS,[10] and ZnO.[11] During the photon-to-electricity conversion in PEC processes, the electron–hole (charge) separation competes with electron–hole recombination, and the net effect largely determines the performance of PEC biosensors.

Semiconductor quantum dots (QDs) are promising agents for biosensors and biomolecule–QD hybrid systems due to their unique electronic and photonic properties.[12] Besides the well-known optical transducers based on fluorescence, the area of QD-based PEC sensors has recently evolved into a rather new and important branch of biosensing.[1b] However, as for other PEC devices, the PEC performance (photocurrent) of QDs is still largely limited by the charge separation efficiency.

Currently, the strategies for increasing the photocurrent in QDs in PEC biosensors are mostly referenced from those explored in photovoltaics and photocatalysis.[13] The first strategy is to fabricate semiconductor QDs with metal nanoparticles to form multicomponent or multiphase heterojunctions.[5a,b] Electron transfer from semiconductor QDs to metal nanoparticles can easily occur through Schottky contact due to the lower Fermi energy of the latter, which facilitates electron–hole separation. The second commonly used strategy is to explore type II heterostructures (in some cases, type II core–shell structures). In such heterostructures, the electron and hole are spatially localized, thus resulting in increased separation efficiency. A typical example of such a heterostructure is TiO_2-CdS.[5c,14] The third popular approach is to extract the photoexcited electrons from QDs with carbon materials, most notably carbon nanotubes (CNTs) and graphene. Due to the high

[a] Dr. P. Wu, Dr. J.-B. Pan, X.-L. Li, Prof. J.-J. Xu, Prof. H.-Y. Chen
State Key Laboratory of Analytical Chemistry for Life Science
School of Chemistry and Chemical Engineering
Nanjing University, Nanjing 210093 (China)
E-mail: xujj@nju.edu.cn
hychen@nju.edu.cn

[b] Dr. P. Wu, Prof. X. Hou
Analytical & Testing Center
Sichuan University
Chengdu 610064 (China)

[c] Prof. H.-Y. Chen
Collaborative Innovation Center of Functionalized Probes
for Chemical Imaging in Universities of Shandong
Shandong Normal University
Jinan 250014 (China)

Supporting information for this article is available on the WWW under http://dx.doi.org/10.1002/chem.201405798.

electron mobility in CNTs or graphene, photoexcited electrons transferred from the semiconductor conduction band (CB) to graphene are easily separated from the surface of the QDs, as is seen in graphene-CdS[6c,15] and CNTs-CdS.[16] These strategies are clearly focused on interfacing QDs with other materials for improved charge carrier separation. The intrinsic exciton process of QDs, namely electron and hole relaxation pathways, on the other hand, is seldom taken into account.[17]

Transition metal ion doping has long been considered as an effective means of modifying the electronic and photophysical properties of QDs.[18] Upon doping, the dopant creates electronic states in the mid-gap region of the QD, which alter the electron–hole separation and recombination dynamics. Mn^{2+}-doping is by far the most studied system, whereby the emission of QDs occurs at around 585 nm due to the Mn^{2+} d–d transition ($^4T_1 \rightarrow {}^6A_1$).[19] Most importantly, this transition is both spin and orbitally forbidden, resulting in an ms-scale lifetime that is about 10^4–10^5-fold slower than in the case of undoped QDs (ns-scale).[18] In other words, the slowed recombination dynamics will result in more opportunities for electron–hole separation. However, this intrinsic property of doping has seldom been explored for PEC biosensor fabrication.

Therefore, we propose herein the use of Mn-doped CdS QDs for PEC biosensor fabrication (Scheme 1). Upon excitation of

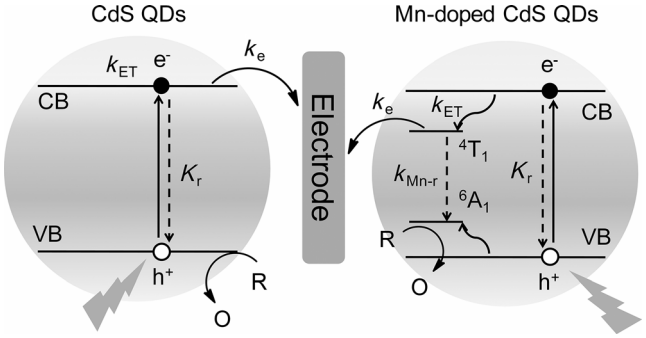

Scheme 1. Schematic illustration of the basic process of electron–hole generation, recombination, and separation in electrodes modified with CdS QDs and Mn-doped CdS QDs upon excitation (not to scale). K_r is the rate of the recombination pathway between the conduction band (CB) and valence band (VB), K_e is the electron-transfer rate from the QDs to the electrode, K_{ET} is the interdot electron-transfer rate from the CB to the Mn^{2+} $^4T_1$ band, and $K_{Mn\text{-}r}$ is the rate of the recombination pathway between the Mn^{2+} $^4T_1$ band and the $^6A_1$ band.

undoped CdS QDs, the electrons in the CB can either be tunneled to the electrode (with rate constant K_e) or recombine with holes in the valence band (VB; with rate constant K_r). For Mn-doped CdS QDs, however, after excitation, electrons in the CB and holes in the VB will be first transferred to the Mn^{2+} $^4T_1$ band and $^6A_1$ band, respectively (with rate constant K_{ET}). This process is reported to proceed on a ps-timescale.[20] Electrons in the Mn^{2+} $^4T_1$ band can either be transferred to the electrode (K_e) or recombine with holes in the $^6A_1$ band ($K_{Mn\text{-}r}$). Accordingly, photocurrent generation is mainly governed by the competition between K_e and K_r (for CdS QDs) or $K_{Mn\text{-}r}$ (for Mn-doped CdS QDs). The long-lived charge carriers in Mn-doped CdS QDs may provide enough time delay to match the related redox-reaction event in solution, which is expected to boost the photocurrent generation. An electrode modified with Mn-doped CdS QDs has been further functionalized for photoelectrochemical cytosensing.

Results and Discussion

PEC performance of Mn-doped CdS QDs

The PEC performance of Mn-doped CdS QDs was first characterized and compared with that of undoped CdS QDs to confirm that the long-lived charge carriers in the Mn-doped system were advantageous for increasing the photocurrent. To facilitate film formation on the electrode and subsequent functionalization, a co-precipitation approach was employed for synthesis of the QDs (see the Supporting Information).[21] Experimentally, the QDs/glassy carbon electrode (GCE) was prepared by drop-casting a solution of QDs onto the electrode and then evaporating the solvent at room temperature to allow the formation of a film of QDs (see the Supporting Information for experimental details). The photocurrent generation of the film was studied using the QDs/GCE as a photoanode and ascorbic acid as a hole scavenger. Figure 1 A depicts the

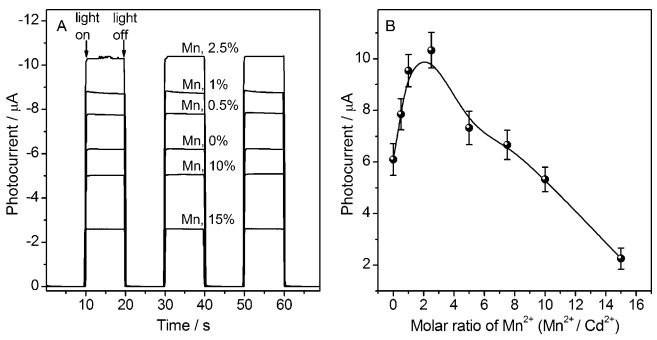

Figure 1. PEC performance of Mn-doped CdS QDs: A) photocurrent response (*i*–t curve) of Mn-doped CdS QDs/GCE, and B) the effect of Mn^{2+} doping amount (molar ratio of Mn^{2+} to Cd^{2+}) on the obtained neat photocurrent. The PEC tests were performed in 0.10 M PBS containing 0.10 M ascorbic acid (AA) at a working potential of 0.0 V and 410 nm excitation wavelength, under nitrogen.

photocurrent responses of CdS QDs and Mn-doped CdS QDs under illumination with light of wavelength 410 nm. Clearly, the photocurrent was improved upon doping with Mn^{2+}, and the maximum increase (about 80%) was observed at a doping level of 2.5% (Figure 1 B), which is very close to the typical doping amount in a previous study of Mn-doped CdS QDs.[22] A further increase in the Mn^{2+} doping amount would presumably result in surface-bound Mn^{2+}, which would quench the excitons in the CdS QDs (Table S1). Since Mn^{2+} can be doped into a series of host QDs with larger band-gaps than that of the Mn^{2+} transition,[23] Mn^{2+}-induced photocurrent increases were also observed in ZnSe QDs and CdSe QDs of appropriate sizes (Figures S1 and S2).

Probing the Mn^{2+} dopant in Mn-doped CdS QDs

Figure 1 demonstrates that the incorporation of Mn^{2+} into CdS QDs led to increased photon-to-electricity efficiency, but whether this increased performance could be attributed to the effect of long-lived charge carriers needed further verification. At a doping level of 2.5%, the color of Mn-doped CdS QDs is almost the same as that of the undoped material (inset in Figure 2A). Absorbance measurements also indicated that the

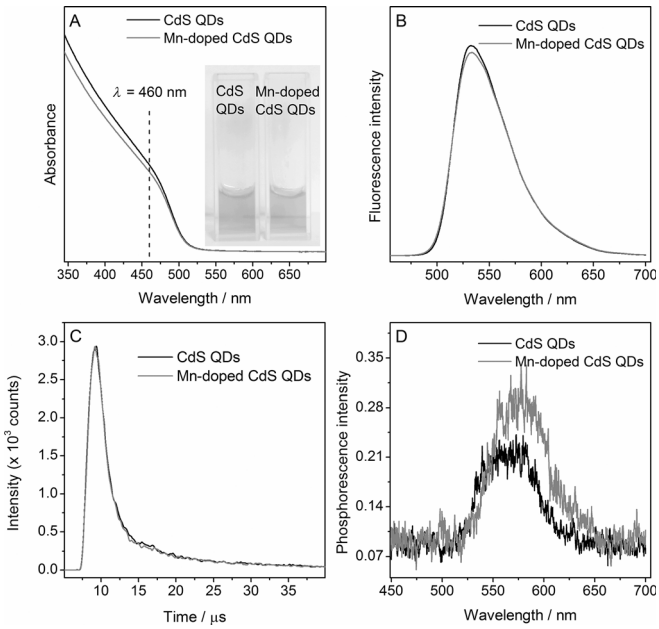

Figure 2. Characterization of the CdS QDs and Mn-doped CdS QDs (doping amount: 2.5%): A) UV/Vis absorption spectra, B) fluorescence emission spectra (λ_{ex} = 380 nm), C) fluorescence decay curves (λ_{ex} = 380 nm, λ_{em} = 540 nm), and D) phosphorescence emission spectra (λ_{ex} = 340 nm). Photographs of the two types of QDs in solution are shown in the inset in Figure 2A.

absorption profiles of CdS QDs and Mn-doped CdS QDs are essentially the same within experimental uncertainty, with a characteristic absorption located at around 460 nm (Figure 2A). TEM images showed that the sizes of the Mn-doped and undoped CdS QDs were both about 5–6 nm (Figure S3), consistent with their absorptions. Both types of QDs exhibited broad, tailed, and weak fluorescence centered at 540 nm (Figure 2B), with fluorescence decays of about 2 μs (Figure 2C). Due to the absence of capping ligands, a large number of surface defects are generated during the co-precipitation synthesis. The fluorescence emission and decay behaviors are characteristic of trap-state emission from CdS QDs.[24]

The above physical characterizations all indicated minimal differences between Mn-doped and undoped CdS QDs, in other words, no sign of Mn^{2+} doping. The most representative characteristic of Mn^{2+} doping, that is, the long-lived emission from the Mn^{2+} d–d transition ($^4T_1 \rightarrow {}^6A_1$), could not be isolated from the broad and tailed fluorescence emission. Nor could it be observed in phosphorescence measurement mode (Figure 2D), as seen for ZnSe QDs (Figure S1), probably due to the quenching effect of surface traps.[12a] For Mn-doped CdS QDs, this weak emission was slightly shifted, probably because of a change in the surface defects upon Mn doping.

To better probe the Mn^{2+} doping, a shell of ZnS was applied to passivate the surface defects of the Mn-doped ZnS QDs (based on the formation of a type I structure for saturation of free valences at the surface of the QDs; for experimental details, see the Supporting Information).[22] The absorption spectra of the CdS QDs and Mn-doped CdS QDs were still similar to one another after applying a ZnS shell (a typical large band-gap material for type I heterostructures; Figure 3A), but the

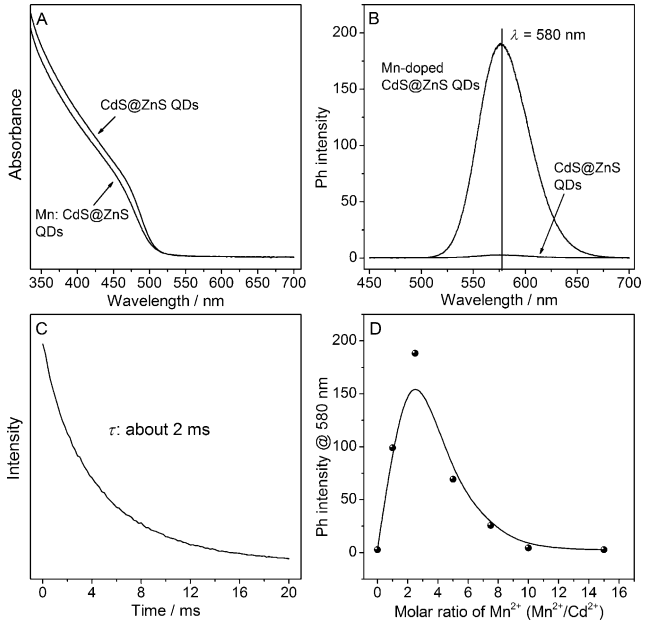

Figure 3. Characterization of the CdS QDs and Mn-doped CdS QDs (doping amount: 2.5%) after ZnS shelling: A) UV/Vis absorption spectra, B) phosphorescence emission spectra (λ_{ex} = 380 nm), C) phosphorescence decay curve (λ_{ex} = 340 nm, λ_{em} = 580 nm), and D) dependence of phosphorescence intensity of Mn-doped CdS QDs on Mn^{2+} doping amount.

characteristic phosphorescence emission from the Mn^{2+} d–d triplet transition ($^4T_1 \rightarrow {}^6A_1$) was clearly observed in phosphorescence measurement mode (Figure 3B), with a decay on an ms timescale (Figure 3C). This provided direct spectroscopic evidence of Mn^{2+} doping.[18] The phosphorescence intensity was maximized at a doping level of 2.5%, which is similar to that used in previous reports.[25] Most importantly, the dependence of the phosphorescence intensity of the Mn-doped CdS QDs on the Mn^{2+} doping amount (Figure 3D) was in excellent agreement with the corresponding dependence of the photocurrent generation (Figure 1B), confirming that the increased photocurrent was truly associated with the Mn^{2+} doping. However, it should be noted that the ZnS-shelled Mn-doped CdS QDs had a typical type I structure, which confined the excitons and deactivated the photocurrent generation (Figure S4).

Since Cd^{2+} and Mn^{2+} are both divalent metal cations, the incorporation of Mn^{2+} into the lattice of CdS QDs is expected to have minimal effect on the charge carrier concentration. The electron tunneling rate (K_e) is mainly controlled by the energy barrier between the QDs and the electrode and the difference

Table 1. Summary of the timescales of various exciton processes.

	CdS QDs	Mn-doped CdS QDs	Ref.
K_e (electron transfer rate from QDs to electrode)		no distinction	
K_r (electron–hole recombination rate of VB and CB)	ns	ns	[26]
K_{ET} (electron transfer from CB of CdS QDs to Mn^{2+} $^4T_1$ band)	–	ps	[20]
$K_{Mn\text{-}r}$ (electron–hole recombination rate of Mn^{2+} $^4T_1$ band and $^6A_1$ band)	–	ms	[26b]

between the Fermi level of the electrode and the energetic bands of the QDs. Because the physical properties of CdS QDs and Mn-doped CdS QDs are essentially indistinguishable (Figure 2) and the electrode preparations are also the same, the charge carrier migration behavior at the interface between QDs and the electrode can be regarded as being the same. The timescale of other exciton processes can be assessed either experimentally ($K_{Mn\text{-}r}$) or from literature reports (K_r and K_{ET}), as indicated in Table 1. As expected, the long-lived charge carriers elicited by Mn^{2+} doping clearly increase electron tunneling from the QDs to the electrode and also increase the probability of holes being reduced by the hole capture agent (here ascorbic acid), thus boosting the photocurrent generation.

Optoelectronic properties of Mn-doped CdS QDs

To better understand the Mn^{2+} dopant-induced optoelectronic modification of CdS QDs, the stability of the photocurrent, the dependence of photocurrent generation on the irradiation wavelength, and the effect of a biased potential were studied in detail for both CdS QDs and Mn-doped CdS QDs as photoanodes. The origin of photocurrent generation was probed by recording the photocurrent at different excitation wavelengths (from an Xe lamp). As shown in Figure 4A, the profile of the photocurrent action spectrum for Mn-doped CdS QDs is similar to that for undoped CdS QDs as well as those for other CdS-based nanocomposites.[6c,16] Moreover, the data revealed that Mn^{2+} doping caused minimal change in the absorption and excitation of the CdS QDs (Scheme 1). Identical reproducible photocurrent responses to ON-OFF light cycles (every 10 s) were observed for both CdS QDs and Mn-doped CdS QDs (Figure 4B, 20 cycles), demonstrating excellent stability for PEC biosensor development.

Figure 4C indicates the dependence of photocurrent generation on the pre-biased potential of the electrode. On increasing the pre-biased potential, the electron energy of the electrode decreases, which facilitates electron transfer from the QDs to the electrode and thus increases the photocurrent. However, further increasing the biased potential resulted in decreased photocurrent, possibly because of prevailing electron–hole recombination. Significantly, the onset potential for photocurrent generation in Mn-doped CdS QDs is somewhat more positive than that in the case of undoped CdS QDs, because the energy level of the Mn^{2+} $^4T_1$ band is lower than the CB of CdS QDs. This phenomenon further validates the electron-transfer pathway in the Mn-doped CdS QDs (from the Mn^{2+} $^4T_1$ band to the electrode).

Application of Mn-doped CdS QDs for the development of a PEC-based biosensor for cancer cell detection

Early detection of carcinoma cells is critically important for clinical diagnostics, toxicity monitoring, and public health protection.[27] As a newly developed analytical technique, PEC-based cytosensors have received great attention in the past few years.[6] On the basis of the efficient PEC performance of Mn-doped CdS QDs, a sensitive cytosensor has been developed for targeted cancer cell capture and detection. For the capture of cancer cells, 3-aminophenylboronic acid (APBA) was employed as the cell-recognizing moiety, on the basis of the specific complexation between boronic acid groups and carbohydrates on cancer cell membranes.[28] The configuration of the designed system and the corresponding PEC process are shown in Scheme 2 (for experimental details, see the Supporting Information). To append APBA, a Mn-doped CdS QDs/GCE was first assembled with 3-mercaptopropionic acid (MPA). After activating the terminal carboxyl groups with *N*-(3-dimethylaminopropyl)-*N*′-ethylcarbodiimide hydrochloride (EDC) and *N*-hydroxysuccinimide (NHS), APBA was attached to the QDs for cancer cell capture. The series of functionalization steps was further confirmed by FTIR analysis (Figure S5). Because cells are insulating entities, cell adhesion on the electrode will increase its impedance, thereby hindering access of the hole scavenger (ascorbic acid in this work) and decreasing the photocurrent.

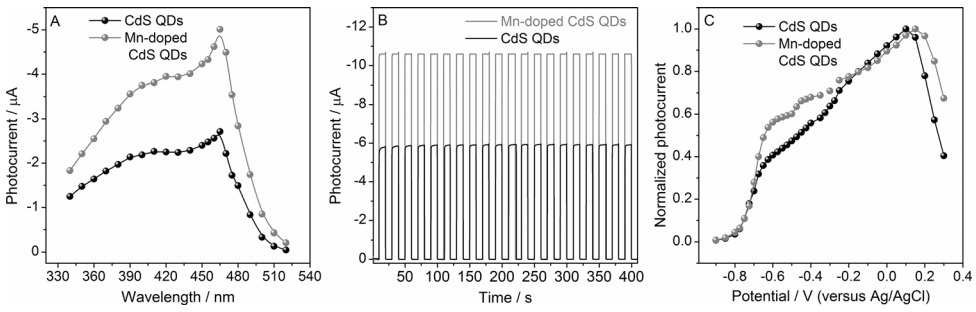

Figure 4. Optoelectronic characterization of the Mn-doped CdS QDs/GCE photoanode: A) Photocurrent action spectra; B) photocurrent stability test when light irradiation was turned on every 10 s; C) influence of the biased potential. All of the PEC tests were performed in 0.10 M PBS containing 0.10 M ascorbic acid (AA) at a working potential of 0.0 V (except D) and 410 nm excitation wavelength, under nitrogen.

The capture of K562 cells by the APBA/Mn-doped CdS QDs/GCE was assessed by microsco-

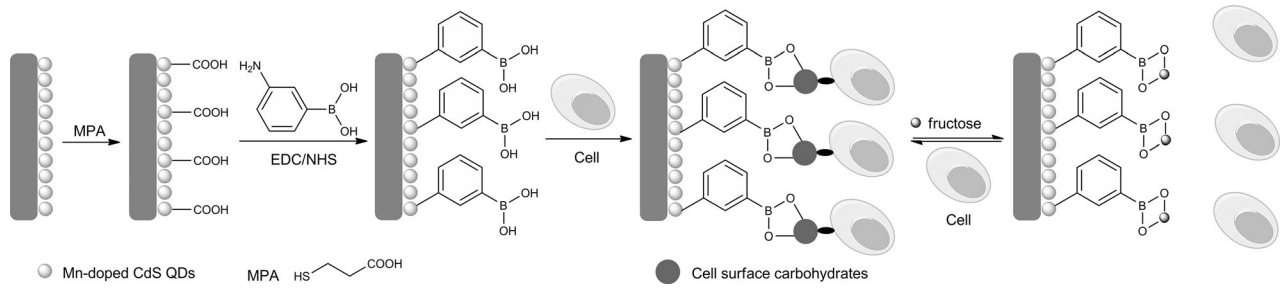

Scheme 2. Functionalization of Mn-doped CdS QDs/GCE for PEC cancer cell detection.

py and electrochemical impedance spectroscopy (EIS). As shown in Figure 5A, without APBA functionalization, no cells were captured. After incubation of the APBA/Mn-doped CdS QDs/GCE with K562 cells for 120 min, numerous cells adhered to the electrode (Figure 5B). Compared to the cells before capture (Figure S6), most of the captured cells were viable, as evidenced by CMAC (a blue CellTracker) staining (Figure 5C). The corresponding EIS change was in accordance with fluorescence microscopic characterization (Figure 5D). The bare GCE showed a low DC resistance to the redox process. After coating with QDs and APBA functionalization, R_{et} increased because the QDs' film hindered access of the redox probe. After adhesion of K562 cells onto the APBA/Mn-doped CdS QDs/GCE, the impedance was further increased owing to the effect of the dielectric behavior of the cells on the interfacial electron transfer.

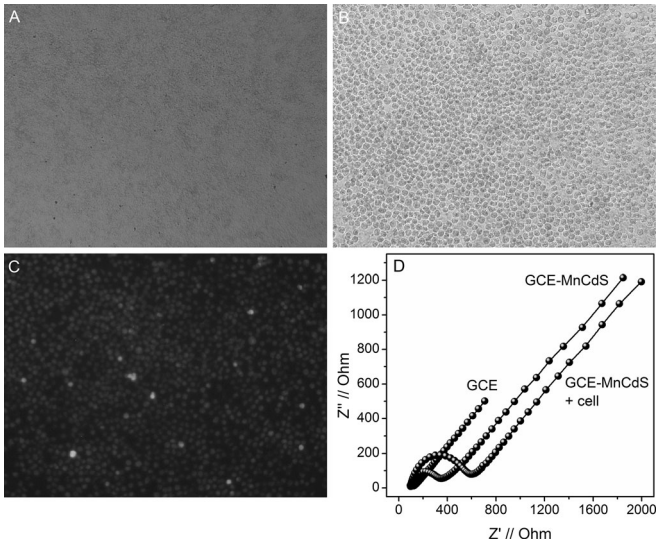

Figure 5. Characterization of cell capture by the APBA/Mn-doped CdS QDs/GCE: A) photo image of the APBA/Mn-doped CdS QDs/GCE, B) bright-field image of cells captured on the APBA/Mn-doped CdS QDs/GCE, C) dark-field fluorescent image of CMAC-stained cells captured on the APBA/Mn-doped CdS QDs/GCE, and D) EIS of the bare GCE and the APBA/Mn-doped CdS QDs/GCE before and after cell capture (3.5×10^6 cells/mL).

After incubation with K562 cells, the photocurrent of the APBA/Mn-doped CdS QDs/GCE decreased. On the basis of this decrease upon the capture of cells, a photoelectrochemical cytosensor was constructed. The decrease in photocurrent intensity was directly related to the number of captured K562 cells. As shown in Figure 6A, the photocurrent of the electrode decreased gradually with increasing number of incubative cells, thereby revealing that the cells were specifically captured by the photosensitive film of the APBA/Mn-doped CdS QDs. Figure 6B shows the linear calibration plot of the decrease in photocurrent versus the logarithm of the K562 cell concentration with the proposed cytosensor. A linear relationship was obtained in the range 3.5×10^2–7.0×10^6 cells/mL. The linear regression equation was ΔI (μA) = 1.26 log C (cells per mL) − 1.44, with a correlation coefficient of 0.9956. The limit of detection (3σ) for K562 cells was estimated to be 200 cells per mL, which is comparable to those for previously reported cytosensors (Table S2).

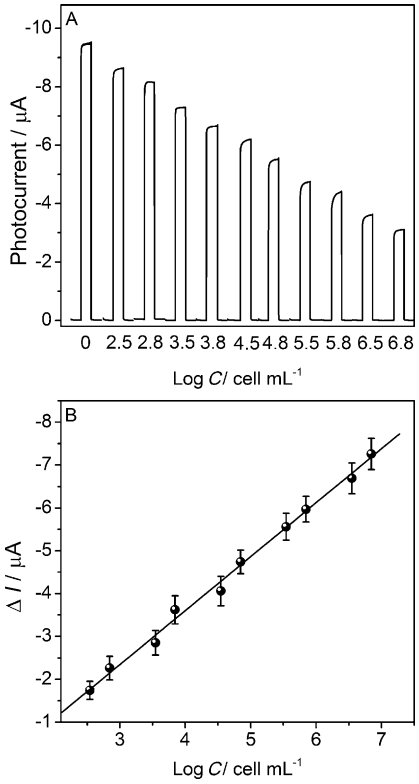

Figure 6. PEC cytosensor for K562 cell detection: A) effect of K562 cell concentration on the photocurrent response, B) calibration plot of photocurrent decrement versus log[cell]. All of the PEC tests were performed in 0.10 M PBS containing 0.10 M ascorbic acid (AA) at a working potential of 0.0 V and 410 nm excitation wavelength, under nitrogen.

Development of a reusable PEC platform for cancer cell detection

APBA is a well-known small sugar-specific ligand, which has a particularly high affinity for fructose in the pH range 7–9. Accordingly, fructose may displace the adhered cells from the electrode surface.[28] As a proof of concept, we demonstrated the capability of the APBA/Mn-doped CdS QDs/GCE to switch between cell capture and release (Scheme 2), that is, to serve as a reusable PEC platform for cancer cell detection. As presented in Figure S3, after exposure to fructose (50 mM), the captured cells were almost completely released from the surface of the modified electrode, accompanied by simultaneous photocurrent recovery (Figure 7A). The modified electrode

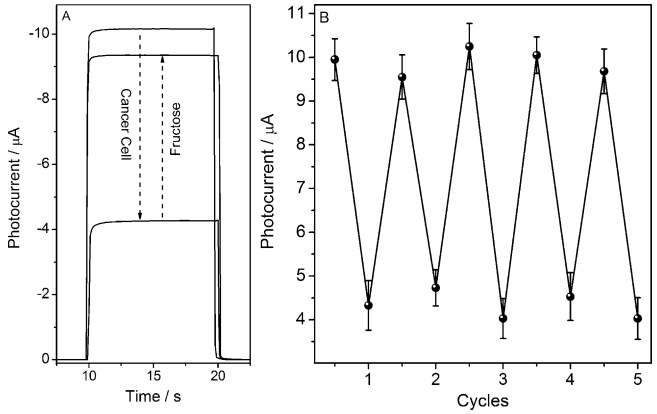

Figure 7. The development of a reusable PEC cytosensor: A) photocurrent responses of the APBA/Mn-doped CdS QDs/GCE upon binding of K562 cells (3.5×10^6 cells per mL) and reconditioning with fructose, B) photocurrent switching cycles between cell capture and release. All of the PEC tests were performed in 0.10 M PBS containing 0.10 M ascorbic acid (AA) at a working potential of 0.0 V and 410 nm excitation wavelength, under nitrogen.

could be re-activated by treatment with acidified PBS (0.10 M, pH 3.6) and then normal PBS (0.10 M, pH 8.5). After reconditioning, the modified electrode could capture K562 cells once more without an appreciable loss of activity (Figure 7A and Figure S7). Figure 7B shows that the proposed APBA/Mn-doped CdS QDs/GCE could switch between cell capture and release cleanly and repeatedly. Therefore, the proposed PEC platform may be explored as a promising reusable cytosensor.

Conclusion

In summary, we have successfully explored the application of long-lived charge carriers generated by Mn^{2+} doping of CdS QDs as a means of improving the output photocurrent. The long-lived charge carriers slow down the recombination of electron–hole pairs, thereby promoting electron transfer to the electrode. It is expected that other dopants (such as Cu^{2+} or Ni^{2+}) that can insert d bands in the host QDs may also create long-lived charge carriers and thereby boost photocurrent generation. For other host QDs (such as ZnSe or CdSe of appropriate size), doping may again provide an effective means of improving the photocurrent generation. The Mn-doped CdS QDs were coated on the surface of a glassy carbon electrode and then functionalized with a cell surface carbohydrate-specific ligand (3-aminophenylboronic acid) to construct a sensitive PEC cytosensor. This PEC cytosensor showed a good photoelectrochemical effect and cell-capture ability, and has been successfully used for the determination of K562 leukemia cells with a wide linear range and a low detection limit. Moreover, the sugar-specific binding property of 3-aminophenylboronic acid moieties on the surface of the cytosensor facilitates a switching function for capture and release of K562 leukemia cells, which has been further explored for the development of a reusable PEC cytosensing platform.

Acknowledgements

We gratefully acknowledge financial support from the Natural Science Foundation of China (Grant nos. 21327902, 21135003, and 21475090). We also wish to thank Dr. Wei-Wei Zhao of the School of Chemistry and Chemical Engineering and Dr. Wenjun Luo of the Department of Physics, Nanjing University, for their helpful discussions.

Keywords: long-lived charge carriers · Mn^{2+} doping · photoelectrochemical biosensing · quantum dots · sensors

[1] a) W.-W. Zhao, J.-J. Xu, H.-Y. Chen, *Chem. Rev.* **2014**, *114*, 7421–7441; b) Z. Yue, F. Lisdat, W. J. Parak, S. G. Hickey, L. P. Tu, N. Sabir, D. Dorfs, N. C. Bigall, *ACS Appl. Mater. Interfaces* **2013**, *5*, 2800–2814; c) W.-W. Zhao, M. Xiong, X.-R. Li, J.-J. Xu, H.-Y. Chen, *Electrochem. Commun.* **2014**, *38*, 40–43; d) F. Wang, X. Q. Liu, I. Willner, *Adv. Mater.* **2013**, *25*, 349–377; e) W.-W. Zhao, J.-J. Xu, H.-Y. Chen, *Chem. Soc. Rev.* **2015**, *44*, 729–741.

[2] a) P. Wang, X. Y. Ma, M. Q. Su, Q. Hao, J. P. Lei, H. X. Ju, *Chem. Commun.* **2012**, *48*, 10216–10218; b) G. L. Wang, J. J. Xu, H. Y. Chen, *Nanoscale* **2010**, *2*, 1112–1114; c) Y. Liang, B. A. Kong, A. W. Zhu, Z. Wang, Y. Tian, *Chem. Commun.* **2012**, *48*, 245–247.

[3] a) J. Tang, B. Kong, Y. C. Wang, M. Xu, Y. L. Wang, H. Wu, G. F. Zheng, *Nano Lett.* **2013**, *13*, 5350–5354; b) Y. T. Long, C. Kong, D. W. Li, Y. Li, S. Chowdhury, H. Tian, *Small* **2011**, *7*, 1624–1628.

[4] a) A. Okamoto, T. Kamei, I. Saito, *J. Am. Chem. Soc.* **2006**, *128*, 658–662; b) W. W. Zhao, P. P. Yu, Y. Shan, J. Wang, J. J. Xu, H. Y. Chen, *Anal. Chem.* **2012**, *84*, 5892–5897; c) X. R. Zhang, Y. Q. Zhao, H. R. Zhou, B. Qu, *Biosens. Bioelectron.* **2011**, *26*, 2737–2741; d) M. M. Liang, S. L. Liu, M. Y. Wei, L. H. Guo, *Anal. Chem.* **2006**, *78*, 621–623.

[5] a) Y. R. An, L. L. Tang, X. L. Jiang, H. Chen, M. C. Yang, L. T. Jin, S. P. Zhang, C. G. Wang, W. Zhang, *Chem. Eur. J.* **2010**, *16*, 14439–14446; b) P. M. Da, W. J. Li, X. Lin, Y. C. Wang, J. Tang, G. F. Zheng, *Anal. Chem.* **2014**, *86*, 6633–6639; c) G. L. Wang, J. J. Xu, H. Y. Chen, S. Z. Fu, *Biosens. Bioelectron.* **2009**, *25*, 791–796.

[6] a) J. Tang, Y. Zhang, B. Kong, Y. Wang, P. Da, J. Li, A. A. Elzatahry, D. Zhao, X. Gong, G. F. Zheng, *Nano Lett.* **2014**, *14*, 2702–2708; b) W. W. Zhao, L. Zhang, J. J. Xu, H. Y. Chen, *Chem. Commun.* **2012**, *48*, 9456–9458; c) X. M. Zhao, S. W. Zhou, L. P. Jiang, W. H. Hou, Q. M. Shen, J. J. Zhu, *Chem. Eur. J.* **2012**, *18*, 4974–4981; d) Z. Qian, H. J. Bai, G. L. Wang, J. J. Xu, H. Y. Chen, *Biosens. Bioelectron.* **2010**, *25*, 2045–2050.

[7] A. E. Becquerel, *C. R. Acad. Sci.* **1839**, *9*, 145–149.

[8] a) A. Ikeda, M. Nakasu, S. Ogasawara, H. Nakanishi, M. Nakamura, J. Kikuchi, *Org. Lett.* **2009**, *11*, 1163–1166; b) A. Kira, T. Umeyama, Y. Matano, K. Yoshida, S. Isoda, J. K. Park, D. Kim, H. Imahori, *J. Am. Chem. Soc.* **2009**, *131*, 3198–3200; c) W. W. Tu, J. P. Lei, P. Wang, H. X. Ju, *Chem. Eur. J.* **2011**, *17*, 9440–9447.

[9] a) M. A. Fox, T. P. Tien, *Anal. Chem.* **1988**, *60*, 2278–2282; b) H. Tokudome, Y. Yamada, S. Sonezaki, H. Ishikawa, M. Bekki, K. Kanehira, M. Miyauchi, *Appl. Phys. Lett.* **2005**, *87*, 213901.

[10] a) R. Baron, C. H. Huang, D. M. Bassani, A. Onopriyenko, M. Zayats, I. Willner, *Angew. Chem. Int. Ed.* **2005**, *44*, 4010 – 4015; *Angew. Chem.* **2005**, *117*, 4078 – 4083; b) H. B. Yildiz, R. Tel-Vered, I. Willner, *Angew. Chem. Int. Ed.* **2008**, *47*, 6629 – 6633; *Angew. Chem.* **2008**, *120*, 6731 – 6735.
[11] a) X. Y. Yang, A. Wolcott, G. M. Wang, A. Sobo, R. C. Fitzmorris, F. Qian, J. Z. Zhang, Y. Li, *Nano Lett.* **2009**, *9*, 2331 – 2336; b) W. W. Zhan, Q. Kuang, J. Z. Zhou, X. J. Kong, Z. X. Xie, L. S. Zheng, *J. Am. Chem. Soc.* **2013**, *135*, 1926 – 1933.
[12] a) E. Petryayeva, W. R. Algar, I. L. Medintz, *Appl. Spectrosc.* **2013**, *67*, 215 – 252; b) W. R. Algar, K. Susumu, J. B. Delehanty, I. L. Medintz, *Anal. Chem.* **2011**, *83*, 8826 – 8837; c) P. Wu, T. Zhao, S. L. Wang, X. D. Hou, *Nanoscale* **2014**, *6*, 43 – 64.
[13] R. Marschall, *Adv. Funct. Mater.* **2014**, *24*, 2421 – 2440.
[14] W. W. Zhao, Z. Y. Ma, D. Y. Yan, J. J. Xu, H. Y. Chen, *Anal. Chem.* **2012**, *84*, 10518 – 10521.
[15] C. X. Guo, H. B. Yang, Z. M. Sheng, Z. S. Lu, Q. L. Song, C. M. Li, *Angew. Chem. Int. Ed.* **2010**, *49*, 3014 – 3017; *Angew. Chem.* **2010**, *122*, 3078 – 3081.
[16] I. Robel, B. A. Bunker, P. V. Kamat, *Adv. Mater.* **2005**, *17*, 2458 – 2463.
[17] P. K. Santra, P. V. Kamat, *J. Am. Chem. Soc.* **2012**, *134*, 2508 – 2511.
[18] a) N. Pradhan, D. D. Sarma, *J. Phys. Chem. Lett.* **2011**, *2*, 2818 – 2826; b) P. Wu, X.-P. Yan, *Chem. Soc. Rev.* **2013**, *42*, 5489 – 5521; c) D. J. Norris, A. L. Efros, S. C. Erwin, *Science* **2008**, *319*, 1776 – 1779.
[19] a) Y. He, H.-F. Wang, X.-P. Yan, *Anal. Chem.* **2008**, *80*, 3832 – 3837; b) R. N. Bhargava, D. Gallagher, X. Hong, A. Nurmikko, *Phys. Rev. Lett.* **1994**, *72*, 416 – 419; c) N. Pradhan, X. G. Peng, *J. Am. Chem. Soc.* **2007**, *129*, 3339 – 3347; d) A. Nag, S. Chakraborty, D. D. Sarma, *J. Am. Chem. Soc.* **2008**, *130*, 10605 – 10611.
[20] H. Y. Chen, T. Y. Chen, D. H. Son, *J. Phys. Chem. C* **2010**, *114*, 4418 – 4423.
[21] Y. Shan, J.-J. Xu, H.-Y. Chen, *Chem. Commun.* **2009**, 905 – 907.
[22] a) H. Yang, P. H. Holloway, *Appl. Phys. Lett.* **2003**, *82*, 1965 – 1967; b) H. Yang, P. H. Holloway, *Adv. Funct. Mater.* **2004**, *14*, 152 – 156.
[23] R. Beaulac, P. I. Archer, X. Y. Liu, S. Lee, G. M. Salley, M. Dobrowolska, J. K. Furdyna, D. R. Gamelin, *Nano Lett.* **2008**, *8*, 1197 – 1201.
[24] A. Nag, S. Sapra, C. Nagamani, A. Sharma, N. Pradhan, S. V. Bhat, D. D. Sarma, *Chem. Mater.* **2007**, *19*, 3252 – 3259.
[25] G. Counio, T. Gacoin, J. P. Boilot, *J. Phys. Chem. B* **1998**, *102*, 5257 – 5260.
[26] a) W. Lü, Y. Tokuhiro, I. Umezu, A. Sugimura, Y. Nagasaki, *Appl. Phys. Lett.* **2006**, *89*, 143901; b) A. Ishizumi, Y. Kanemitsu, *Adv. Mater.* **2006**, *18*, 1083 – 1085.
[27] Q. J. Liu, C. S. Wu, H. Cai, N. Hu, J. Zhou, P. Wang, *Chem. Rev.* **2014**, *114*, 6423 – 6461.
[28] a) X. Zhong, H. J. Bai, J. J. Xu, H. Y. Chen, Y. H. Zhu, *Adv. Funct. Mater.* **2010**, *20*, 992 – 999; b) H. L. Liu, Y. Y. Li, K. Sun, J. B. Fan, P. C. Zhang, J. X. Meng, S. T. Wang, L. Jiang, *J. Am. Chem. Soc.* **2013**, *135*, 7603 – 7609.

Received: October 23, 2014
Published online on ■■ ■■, 0000

FULL PAPER

Photoelectrochemical Cytosensor

P. Wu, J.-B. Pan, X.-L. Li, X. Hou, J.-J. Xu, H.-Y. Chen**

■■ – ■■

Long-Lived Charge Carriers in Mn-Doped CdS Quantum Dots for Photoelectrochemical Cytosensing

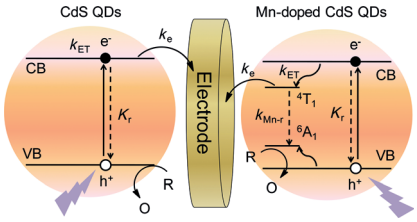

Impeded recombination for enhanced separation: Long-lived charge carriers elicited by Mn^{2+} doping of CdS quantum dots (QDs) boost photocurrent generation therein (see figure). This enhancement has been exploited for photoelectrochemical cytosensing.